Journal of Catalysis 290 (2012) 126–137

Contents lists available at SciVerse ScienceDirect

Journal of Catalysis

journal homepage: www.elsevier.com/locate/jcat

In situ XPS study of methanol reforming on PdGa near-surface intermetallic phases

Christoph Rameshan [a,b], Werner Stadlmayr [a], Simon Penner [a], Harald Lorenz [a], Lukas Mayr [a], Michael Hävecker [b], Raoul Blume [b], Tulio Rocha [b], Detre Teschner [b], Axel Knop-Gericke [b], Robert Schlögl [b], Dmitry Zemlyanov [c], Norbert Memmel [a], Bernhard Klötzer [a,*]

[a] Institute of Physical Chemistry, University of Innsbruck, Innrain 52a, A-6020 Innsbruck, Austria
[b] Department of Inorganic Chemistry, Fritz-Haber-Institute of the Max-Planck-Society, Faradayweg 4–6, D-14195 Berlin, Germany
[c] Purdue University, Birck Nanotechnology Center, 1205 West State Street, West Lafayette, IN 47907-2057, USA

ARTICLE INFO

Article history:
Received 25 October 2011
Revised 2 March 2012
Accepted 11 March 2012
Available online 12 April 2012

Keywords:
PdGa near-surface intermetallic phase
Methanol dehydrogenation
Methanol steam reforming
Oxidative steam reforming
Water activation
Ambient-pressure XPS
In situ spectroscopy

ABSTRACT

In situ X-ray photoelectron spectroscopy and low-energy ion scattering were used to study the preparation, (thermo)chemical and catalytic properties of 1:1 PdGa intermetallic near-surface phases. Deposition of several multilayers of Ga metal and subsequent annealing to 503–523 K led to the formation of a multi-layered 1:1 PdGa near-surface state without desorption of excess Ga to the gas phase. In general, the composition of the PdGa model system is much more variable than that of its PdZn counterpart, which results in gradual changes of the near-surface composition with increasing annealing or reaction temperature.

In contrast to near-surface PdZn, in methanol steam reforming, no temperature region with pronounced CO_2 selectivity was observed, which is due to the inability of purely intermetallic PdGa to efficiently activate water. This allows to pinpoint the water-activating role of the intermetallic/support interface and/or of the oxide support in the related supported Pd_xGa/Ga_2O_3 systems, which exhibit high CO_2 selectivity in a broad temperature range. In contrast, corresponding experiments starting on the purely bimetallic model surface in oxidative methanol reforming yielded high CO_2 selectivity already at low temperatures (~460 K), which is due to efficient O_2 activation on PdGa. In situ detected partial and reversible oxidative Ga segregation on intermetallic PdGa is associated with total oxidation of intermediate C_1 oxygenates to CO_2.

1. Introduction

In recent years, a group of Pd-based catalysts has been studied in search of possible alternatives to selective but sinter-unstable Cu/ZnO catalysts for use in efficient hydrogen production by methanol steam reforming [1–3]. It is widely accepted that the active and CO_2-selective state of these catalysts at least requires the presence of a single bimetallic (Pd–Zn, Pd–Ga or Pd–In), induced by reductive activation in the temperature region 523–773 K [1–3]. By far, the most studied of these catalysts is the PdZn/ZnO system, which is already scrutinized in many structural, electronic and catalytic aspects [1–10]. A 1:1 PdZn intermetallic phase has been proven to be essential, as has been the role of the oxidized Zn centers and their interaction with the intermetallic surface for efficient water activation [9,10]. Despite the striking catalytic similarities between the three systems (for all of the supported bimetallic systems a CO_2-selective temperature region has been verified), key parameters of the Pd–Ga (and the related Pd–In) system are still far from clear. Structure-wise, this refers in the first place to the question, if also a 1:1 PdGa near-surface intermetallic phase (in the following abbreviated as "NSIP") can be prepared in a similar way as PdZn and if this isolated bimetallic exhibits not only comparable catalytic properties, but also comparable thermal and thermochemical stability. This will moreover connect to previous structural and sintering studies on oxide-supported bimetallic Pd_xGa particles, where an – in comparison with PdZn – less-pronounced thermal stability and generally a higher amount of sintering have been observed [11,12]. For a direct comparison with Pd_1Zn_1, the Pd–Ga phase diagram reveals that the Pd_1Ga_1 intermetallic is one of the stable, but not the thermodynamically most stable compound, which is clearly the case for Pd_1Zn_1 [13]. The Pd_1Ga_1 bulk intermetallic compound is, however, stable over a wide range of temperatures and exhibits a FeSi crystal structure. It can be regarded as a distorted NaCl structure with increased coordination number from 6 to 7. Each Pd atom is therefore surrounded by 7 Ga atoms (3 + 3 + 1) [14]. Thermodynamically, the formation of stable intermetallic compounds can be explained on the basis of considerable enthalpies of formation [15]. The energetically favorable Pd–Ga interaction can be understood on the basis

* Corresponding author. Fax: +43 512 507 2925.
E-mail address: Bernhard.Kloetzer@uibk.ac.at (B. Klötzer).

0021-9517
http://dx.doi.org/10.1016/j.jcat.2012.03.009

of strong, localized and covalent Pd–Ga bonds [16]. The alteration of the Pd coordination in Pd_1Ga_1 (as well as in Pd_3Ga_7 and Pd_2Ga) thus also leads to a strong modification of the electronic structure around the Fermi level in comparison with elemental Pd. The XPS spectra of, for example, $Pd_1Ga_1(1\,1\,0)$ are dominated by features between 2 and 5 eV below E_F, attributed to localized Pd-4d states [17]. This electronic modification, in combination with the structural isolation of active Pd sites, gives rise to the excellent catalytic ethene semihydrogenation properties described, for example, in [18].

With respect to a potential methanol reforming application, the most CO_2-selective and CO_2-active oxide-supported bimetallic species is the Pd_2Ga phase-supported on β-Ga_2O_3 [1,11], which is comparably CO_2 active and selective as PdZn/ZnO. The Ga-richer 1:1 phase, also supported on β-Ga_2O_3, has been previously determined to be more affected by SMSI effects and oxidative segregation under reaction conditions and thus to be less selective and active in methanol steam reforming. Nevertheless, Pd_1Ga_1/β-Ga_2O_3 has been shown to be still more CO_2 active and selective than pure β-Ga_2O_3 [11].

Secondly, the selectivity spoiling role of the inverse water–gas shift reaction on the β-Ga_2O_3 support, based on the capability of oxygen vacancy sites to activate water, has already been assessed [11,19]. Although some similarities between ZnO and Ga_2O_3 especially regarding water activation exist [19], it is not per se clear how the – for a high CO_2 selectivity essential – water activation works on the supported Pd_xGa/β-Ga_2O_3 systems.

Partly fueled by previous experiments on the structure and the catalytic properties of supported Pd_1Ga_1 and Pd_2Ga bimetallic particles, which revealed temperature regimes with structurally stable Pd–Ga intermetallic compounds and, for the latter, a particularly high CO_2 selectivity, the present contribution aims at a thorough characterization of the "isolated" Pd–Ga intermetallic surface without contact to the β-Ga_2O_3 support, either to assess a potential analogy to the bi-functional activity of the multi-layered Pd_1Zn_1 NSIP [9,10] or to reveal a possible bi-functional synergism of the Pd–Ga intermetallic surface and the oxide support. In this context, we were particularly interested in a potential role of the oxide's defect chemistry in activating water for the full methanol reforming process toward CO_2. Moreover, an exclusive role of a specific bimetallic surface composition (as already proven for the related Pd_1Zn_1 multilayer NSIP case [9,10]) remained to be verified or disproved. Two types of reforming reactions were studied in situ, namely "water-only" methanol steam reforming (MSR), corresponding to the "ideal" reaction $CH_3OH + H_2O \rightarrow CO_2 + 3H_2$, and oxidative steam reforming (OSR), whereby a certain added amount of O_2 may give rise to H_2-formation stoichiometries ranging from partial methanol oxidation ($CH_3OH + 1/2\ O_2 \rightarrow CO_2 + 2H_2$) to total oxidation ($CH_3OH + 3/2\ O_2 \rightarrow CO_2 + 2H_2O$).

2. Experimental

2.1. Innsbruck experimental setup

The UHV system with attached all-glass high-pressure reaction cell [20] is designed for catalytic studies up to 1 bar on a larger piece of 1.8 cm × 2 cm polycrystalline Pd foil, allowing us to detect reaction products and even minor intermediates with high sensitivity, either by discontinuous sample injection into the gas chromatography–mass spectrometry (GC–MS) setup (HP G1800A) or by direct online MS analysis of the reaction mixture via a capillary leak into the GC/MS detector. The system consists of an UHV chamber with a long-travel Z-manipulator and a small-volume Pyrex glass reactor (52 ml, no hot metal components) attached to the outside of the UHV chamber and accessible via a sample transfer port. The UHV chamber is equipped with an XPS/Auger/ISS spectrometer (Thermo Electron Alpha 110) and a standard double Mg/Al anode X-ray gun (XR 50, SPECS), an Omicron ISE 100 ion gun to provide the focused 1 keV He^+ ions for ISS, an electron beam heater, an ion sputter gun and a mass spectrometer (Balzers). All ISS experiments were performed at an angle of beam incidence $\Psi = 45°$ and a scattering angle of $\vartheta = 90°$, and after correction for the different cross-sections, intensity normalization of the Pd and Ga signals was performed relative to the total backscattering yield, that is, I_{Ga}(normalized) = $I_{Ga}/(I_{Pd} + I_{Ga})$ and I_{Pd}(normalized) = $I_{Pd}/(I_{Pd} + I_{Ga})$. The Pd and Ga scattering cross-sections valid for our specific setup were determined by measurement of the clean Pd foil and a sufficiently thick pure Ga metal surface layer covering all Pd under identical experimental conditions. For controlled Ga deposition, a home-built Ga evaporator was attached, which consists of a small boron nitride crucible filled with Ga metal (99.999%, Goodfellow) and heated by electron bombardment. A water-cooled quartz crystal microbalance monitored the amount of deposited Ga.

The UHV-prepared samples are thereafter transferred by means of a magnetically coupled transfer rod from the UHV sample holder to a Pyrex glass sample holder used inside the all-glass reaction cell. With this all-glass setup of the ambient-pressure reaction cell, no wires or thermocouples are connected to the sample during catalytic measurement (thermocouple mechanically contacted at the outside). Accordingly, background (blind) activity of the reaction cell is routinely checked and was found to be negligible for all tests. A detailed graphic representation of the ambient-pressure reaction cell setup is provided in the Supplementary material (Fig. S1).

The main chamber is pumped by a turbomolecular pump, an ion getter pump and a titanium sublimation pump to a base pressure in the low 10^{-10} mbar range. High purity gases (H_2, O_2, Ar: 5.0) were used as supplied from Messer–Griesheim and dosed via UHV leak valves. The high-pressure cell is evacuated sequentially by a rotary pump (via LN_2 cooled zeolite trap) and then via the main chamber down to UHV base pressure and can be heated from outside to 723 K with an oven covering the cell. For better mixing of the reactants, the high-pressure cell is operated in circulating batch mode. By using an uncoated GC capillary attached to the high-pressure cell, the reaction mixture in the close vicinity of the sample is analyzed continuously by the electron ionization detector (EID) of the GC/MS system. For quantitative measurement of H_2, we used (in parallel with the EID) an additional Balzers QMA 125 detector specifically tuned for optimum H_2 detection. EID and QMS signals of methanol, CO_2, CO, H_2 and CH_2O were externally calibrated and corrected for fragmentation (that is, CO and CH_2O fragments for methanol, CO fragment for CO_2).

A polycrystalline palladium foil (Goodfellow, purity 99.999%, 0.125 mm thick, size 3.5 cm^2) was cleaned on both sides by successive cycles of Ar^+ ion bombardment (6.0×10^{-5} mbar Ar, 503 eV, 1 μA sample current), oxidation (5.0×10^{-7} mbar O_2, $T = 1000$ K), and annealing in hydrogen (5.0×10^{-7} mbar H_2, $T = 700$ K) and in vacuum ($T = 1000$ K) until no impurities were detected by AES and XPS. Details of the preparation of the PdGa multilayer intermetallic phase will be given in Section 3.1. Methanol and methanol/water mixtures were degassed by repeated freeze-and-thaw cycles. All MSR reactions were conducted with methanol/water mixtures of a 1:10 composition of the liquid phase. This corresponds to a room temperature partial pressure ratio of methanol/water = 1:2, as verified by mass spectrometry.

The catalytic experiments were performed in a temperature-programmed manner, that is, the reaction cell was heated at a constant linear rate of ~8 K/min to the final temperature of 623 K, and then kept isothermal at this temperature for ~20 min. Experimental details will be given in context with the individual reaction runs. The advantage of the TPR (temperature-programmed reaction) runs is that pronounced selectivity changes can be monitored

via the partial pressure changes as a function of the reaction temperature, yielding useful qualitative information about changes of the reaction mechanism and the catalyst state. From the product partial pressures vs. time plots the reaction rates were obtained by differentiation and are usually given in partial pressure change per minute [mbar/min], but whenever desired, the turnover frequencies (TOF's) given in molecules per site and second [site^{-1} s^{-1}] can be calculated by multiplication of the partial pressure change with a factor $f = 2.4$, for example, a reaction rate of 1 mbar/min corresponds to a TOF of 2.4 site^{-1} s^{-1} (one site corresponds to a single Pd surface atom on the respective foil substrate; see below). The conversion factor is based on the partial pressures of the reaction products already corrected for the temperature change in the reaction cell during the TPR run and for the steady removal of a fraction of the reaction mixture through the capillary leak. The correction has been achieved by adding 30 mbar Ar inert gas at the beginning of the reaction run and monitoring the $m/z = 40$ Ar intensity throughout the whole experiment. The Ar intensity over time then was used to recalculate the changes of the molar amounts of all products and reactants as referred to the initial state (before TPR start, reactor volume 60.6 ml and 300 K in the whole re-circulating batch system). The total number of potential catalytic surface sites for the clean Pd foil $N_s = 1 \times 10^{16}$ was determined from the Pd surface (area 7 cm^2) being composed of equally distributed (1 1 1) and (1 0 0) facets. To derive TOF numbers on a sample with Pd:Ga = 1:1 surface composition, this number was divided by 2.

2.2. HZB/BESSY II experimental setup

The HZB/BESSY II system [21] (at beamline ISISS-PGM) allowed us to perform in situ photoelectron spectroscopy up to 1 mbar total reactant pressures. It is equipped with differentially pumped electrostatic lenses and a SPECS hemispherical analyzer. The sample is positioned inside the high-pressure/analysis chamber ~2 mm away from a 1 mm aperture, which is the entrance to the lens system separating gas molecules from photoelectrons. Binding energies (BEs) were generally referred to the Fermi edge recorded after each core level measurement. Samples were mounted on a transferable sapphire holder. The temperature was measured by a K-type Ni/NiCr thermocouple spot-welded to the side of the sample, and temperature-programmed heating was done by an IR laser from the rear. Sample cleaning procedures consisted of repeated cycles of Ar^+ sputtering at room and elevated temperatures, annealing up to 950 K in UHV, and exposure to O_2, followed by flashing at 950 K for 60 s in UHV. The cleanliness of the Pd foil substrate was checked by XPS. The sensitivity of the simultaneous MS detection of the reaction products at HZB/BESSY II was not sufficient to extract reliable reaction rate and selectivity data for H_2/CO/CH_2O/CO_2, mainly because of an unfavorable ratio of the large total reactant flow through the XPS high-pressure cell (which is generally operated in constant flow mode) relative to the minor amounts of products formed on the low surface area catalyst (only 0.5 cm^2 PdGa intermetallic compound phase on Pd foil or Pd(1 1 1)). However, "connecting" experiments performed in the Innsbruck setup using the same conditions with respect to initial reactant pressures, PdGa NSIP preparation and reaction temperature range, allowed to assess a possible "pressure gap" effect and provided a reliable connection between the data obtained in either experimental setup.

3. Results and discussion

3.1. Preparation and characterization of the Pd_1Ga_1 NSIP

Similarly to the PdZn system, a thoroughly characterized and reproducible initial bimetallic state is a prerequisite for meaningful catalytic measurements. To reproducibly prepare a Pd_1Ga_1 NSIP, calibration of a monolayer equivalent (MLE) deposited amount of Ga metal is necessary. As Zn and Ga exhibit similar atomic masses (65.4 vs. 69.7 amu), our previous calibration of the quartz microbalance for Zn deposition [9,10] could be easily adapted to Ga deposition. Accordingly, as all other experimental deposition parameters were equivalent, deposition of 22.5 Hz corresponds to 1 MLE of Ga, based on a Pd atom density of 1.4×10^{15} surface Pd-atoms/cm^2 (the average of evenly distributed (1 1 1) and (1 0 0) facets). To back up this calibration, Ga metal was stepwise (in 10 Hz steps) deposited with constant rate on the clean Pd foil at 300 K. Thereafter, LEIS using He^+ ions (1 keV) was performed and complemented by a second series of LEIS measurements with intermediate annealing to 523 K after each Ga deposition.

Fig. 1 shows the corresponding effects. Briefly anticipating the 298 K XPS spectra of Fig. 3, a strong Ga–Pd interaction (intermixing) already after room temperature Ga deposition is evident. The Pd3d shift clearly indicates partial NSIP formation, as evidenced by the high Pd3d BE of 336.15 eV and the "Cu-like" valence band region. For comparison, the BE of Pd3d in clean Pd foil is found at ~335.1 eV, and a high "d-band" induced density of states at the Fermi edge is to be expected on clean Pd.

In Fig. 1, major surface composition changes occur between 0 and 1 MLE (22.5 Hz) Ga (irrespective of the temperature); thereafter, only a slow increase in the Ga surface fraction from ~66% up to 86% is visible at 298 K. In contrast, after 523 K annealing a constant 1:1 ratio is obtained at all depositions beyond 1 MLE, independent of the extra Ga amount beyond 1 MLE. Taken together, a similar situation to the Pd_1Zn_1 NSIP growth process described in [8–10] is likely: at 298 K incomplete alloying leads to a particularly high Ga coordination of the top Pd layers by a combination of partial Pd–Ga intermixing within the surface layer(s) but also extra Ga adsorbed on top of this state, leading to a maximum Pd3d high BE shift in the uppermost region in combination with surface Ga enrichment relative to Pd in LEIS. This can explain the ~66:34 Ga/Pd ratio monitored by LEIS after deposition of 1 MLE Ga at 298 K, which can be converted to a 50:50 ratio by thermal annealing at ~523 K, likely leading to a "bilayered" 1:1 NSIP, in close analogy to bilayered PdZn [8]. We conclude that multilayer Ga depositions exceeding 1 MLE Ga, followed by annealing at ~503–523 K, lead to the respective multi-layered states of the

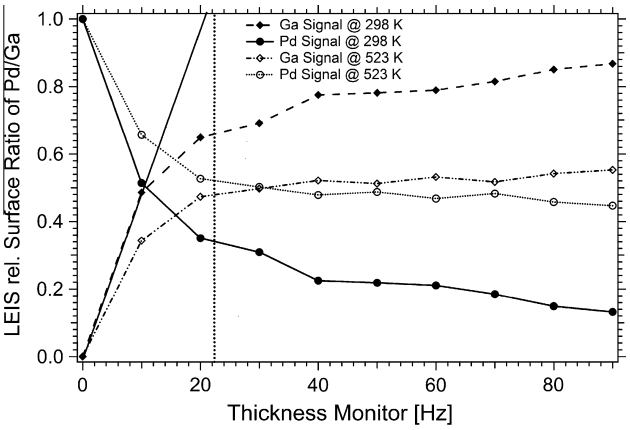

Fig. 1. LEIS-determined ratio of Pd to Ga in the surface using 1 keV He^+ ions plotted vs. the resonant frequency of the quartz crystal in the film thickness monitor. Measurement series with step-wise Ga deposition at 298 K (solid lines) and second series with intermediate tempering at 523 K (dotted lines) prior to analysis. Vertical dashed line: 22.5 Hz Ga metal deposition corresponding to 1 MLE of Ga, based on a Pd surface atom density of 1.4×10^{15} Pd atoms per cm^2. The intersection of the tangential to the 298 K uptake curve with the *X*-axis provides an additional hint for the correctness of the coverage calibration.

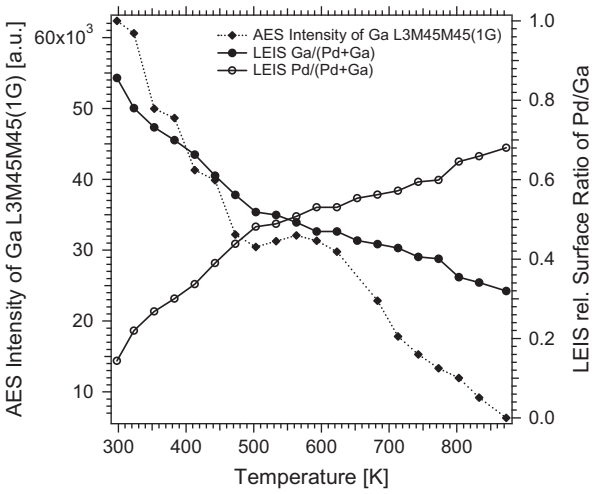

Fig. 2. Ga and Pd surface fractions starting from 4 MLE deposited Ga metal, as determined by LEIS and via Peak-to-Peak intensity of the differentiated Ga–$L_3M_{45}M_{45}$ Auger signal, as a function of the annealing temperature.

Pd_1Ga_1 NSIP with variable thickness. This picture was further corroborated by XPS-depth profiling, showing only little changes of the relative Ga concentration between ~5 and ~13 Å information depth after deposition of 4 MLE Ga and 523 K annealing.

As the Pd_1Ga_1 NSIP was initially intended to be a model system for bulk (FeSi-type) Pd_1Ga_1, we must address the question of potential structural and electronic differences. The 3-dimensional structure within the film has been studied recently by impact-collision ion scattering (ICISS) after 523 K annealing of several MLE Ga [22], revealing an fcc (Pd metal-like) coordination geometry of Pd and Ga which is quite similar to that observed for the multi-layered PdZn NSIP. Thus, a 1:1 coordination chemistry similar to the PdZn NSIP (down to ~13 Å information depth) could be established and closely related MSR properties were initially suspected.

As the structural identity of NSIP and bulk phase was equally not given in case of the Pd_1Zn_1, but nevertheless the Pd_1Zn_1-NSIP was found to be a highly CO_2-selective model system in a certain range of reaction temperature [9,10], the structural differences must not necessarily represent a major obstacle in the Pd_1Ga_1 NSIP case. At least in view of electronic structure, as can be seen in Fig. 3, changes of the valence band DOS of Pd by Ga are still strong and the "Cu-like" situation already shown for the multi-layered Pd_1Zn_1 NSIP could be clearly verified also for the Pd_1Ga_1 NSIP case. By comparison of the Pd3d binding energy position of 336.0 eV reported for the bulk Pd_1Ga_1 compound [23] and of 335.6 eV for the more Ga-depleted Pd_2Ga compound [24] with the Pd3d binding energies between 335.9 eV and 335.75 eV determined after thermal annealing of 4 MLE Ga deposited on Pd foil between 473 K and 523 K (see Fig. 3, Section 3.2), an intermediate electronic state and a pronounced "intermetallic compound character" of the fcc-type Pd_1Ga_1 NSIP between bulk Pd_1Ga_1 and bulk Pd_2Ga_1 can be assumed.

3.2. Thermal stability of the Pd_1Ga_1 NSIP

To gain additional insight into the temperature-dependent surface composition and the associated thermal stability of the Pd_1Ga_1 NSIP, 4 MLE Ga were deposited at ~300 K and step-wise annealed to 800 K. The spectroscopic fingerprints were measured using AES and LEIS and the results were corroborated by in situ XPS measurements at HZB/Bessy II.

Fig. 2 shows an immediate sharp decrease in the Ga–$L_3M_{45}L_{45}$ signal up to about ~500 K. This is obviously related to the increased 1:1 NSIP formation with Ga progressing into deeper layers. In contrast to experiments on PdZn, where Zn "on-top" multilayers easily desorbed to the gas phase already at low temperatures (~450 K), the system Pd–Ga shows a quantitative transition of all deposited Ga into the NSIP state. This is inferred from the much lower vapor pressure of Ga, which therefore cannot desorb to the gas phase in the temperature region 300–800 K. If more than 1 MLE Ga is deposited on the Pd foil and subsequently tempered to, for example, 523 K, the entire Ga transforms into the intermetallic state and forms a correspondingly thick 1:1 Pd–Ga layer. The LEIS measurements correspondingly show a strong decrease in the Ga signal between 300 and 500 K until the ~1:1 surface composition is finally reached at ~503 K. Between 503 K and ~623 K, a small plateau region is visible in the Ga–$L_3M_{45}L_{45}$ signal, which seems to indicate a certain stability range of the Pd_1Ga_1

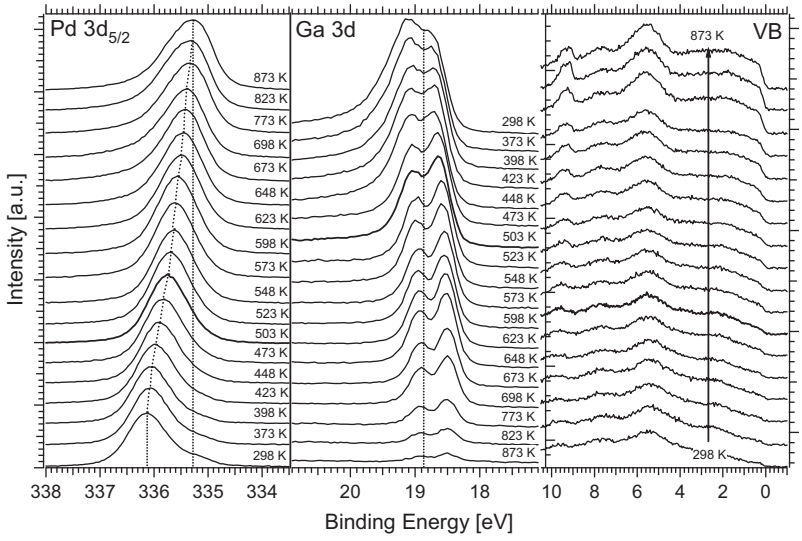

Fig. 3. Temperature-programmed XPS measurements of the Pd $3d_{5/2}$ signal (measured at 470 eV photon energy) and the Ga 3d and valence band signals (measured at 120 eV). Note that the Ga 3d spectra are shown in inverted order as compared to Pd 3d due to the inverse intensity effects. Spectra have been taken in 25 K steps between 373 and 698 K. 4 MLE Ga were initially deposited. For comparison, the BE of Pd3d in clean Pd foil is reported at ~335.1 eV, and a high "d-band" induced density of states at the Fermi edge is to be expected.

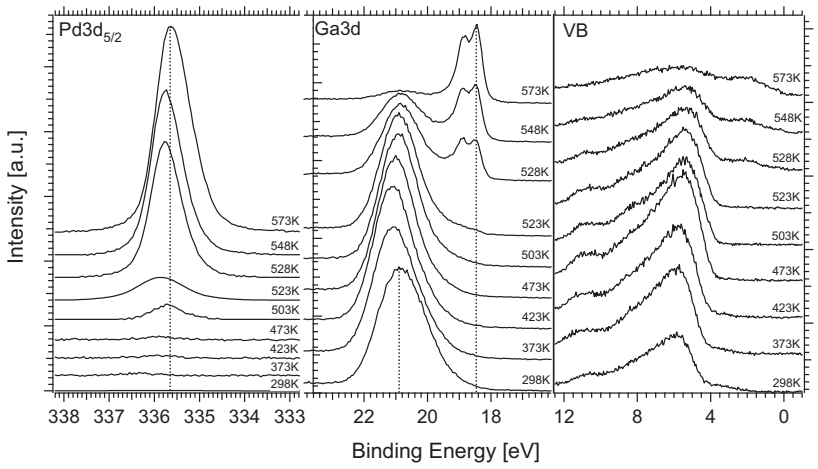

Fig. 4. In situ XPS spectra of the Ga_2O_3-covered Pd foil, prepared by deposition of 4 MLE Ga converted to Ga_2O_3 in 10^{-3} mbar O_2. Subsequent annealing was carried out in 0.1 mbar H_2. Photon energies were the same as in Fig. 4.

NSIP. However, close inspection of the in-parallel measured LEIS spectra indicates changes in surface composition with increasing temperature from ~52:48 at 503 K to ~46:54 Ga:Pd at 623 K. The surface composition hence remains close to 1:1, but small changes due to preferential LEIS-induced sputtering of Ga especially in the top-most layers are likely on the basis of control experiments with variable scattering times. The Auger signal at 1068 eV kinetic energy is less affected by compositional changes in the topmost layers, thus the plateau region is more pronounced. Above ~623 K, the LEIS-derived change of the Pd:Ga ratio is less strong than the related AES intensity drop, and changes almost linearly up to 800 K. As the Ga–$L_3M_{45}L_{45}$ Auger signal decreases much faster than the Ga-LEIS signal, we suspect a PdZn-analogous relative stabilization of the topmost PdGa layer relative to subsurface Ga, as described in [9,10,22]. According to this picture, at higher temperatures rather subsurface Ga than "in-surface" Ga migrates into deeper regions of the Pd bulk and the Pd_1Ga_1 NSIP should thus become specifically diluted in the subsurface region. Accordingly, at 870 K, only the surface composition remains close to Pd_2Ga, meaning that the 870 K state is unfortunately not representative for a Pd_2Ga bulk alloy surface. In summary, the combined data show a relatively stable 1:1 surface and near-surface composition at ~523 K.

To connect to analogous experiments on PdZn, a standard preparation routine for a Pd_1Ga_1 multilayer NSIP has been utilized. ~1, ~2 and ~4 MLE Ga metal were deposited onto the Pd foil and subsequently annealed to 503 K. Ideally, these preparations represent 2, 4 and 8 perfect 1:1 PdGa layers of the Pd_1Ga_1 NSIP, respectively. At this point, it should be noted that angle-resolved LEIS spectra conducted on ~4 MLE Ga on Pd(1 1 1) tempered at 503–523 K did not show the analogous Ga-outward corrugation effects as observed for the multi-layered Pd_1Zn_1 NSIP [9,10,22]. Potential catalytic implications of these structural differences are discussed in Section 3.4.

The above-discussed measurements were in turn complemented by additional in situ XPS experiments at HZB/BESSYII to gain information about the composition of the NSIP vertical to the surface. The experimental conditions were chosen as closely as possible to the ones of the Innsbruck experimental setup (compare Section 2.1). Multilayers of Ga metal (and also of Ga_2O_3, to study the reducibility of the oxide in contact to Pd in hydrogen) were deposited onto the Pd foil and stepwise annealed with in-parallel detection by in situ XPS. Fig. 3 shows the results of these measurements in a three-panel overview, highlighting the Pd $3d_{5/2}$, Ga 3d and valence band (VB) regions. The signals were collected with photon energies of 470 eV (Pd $3d_{5/2}$) and 120 eV (Ga 3d, VB), respectively, to ensure almost identical kinetic energies and hence identical information depth of the electrons.

For the experiments shown in Fig. 3, 4 MLE Ga metal were deposited and the Pd foil subsequently annealed to the indicated temperatures. We note that a small O_2 or H_2O background pressure cannot be avoided in the HZB/BESSY II setup; therefore, the deposition was carried out in 10^{-6} mbar H_2 background pressure to avoid partial oxidation of Ga metal. The Pd $3d_{5/2}$ signal shifts to lower binding energies as the temperature increases, that is, from about 336.15 eV at 298 K to 335.25 eV at 873 K. In analogy to the PdZn system, no distinct stability region is visible in XPS, and the Pd–Ga coordination appears to change in a more or less gradual manner [9]. The 503 K–annealing spectrum indicates the preparation and "initial catalyst" conditions for the subsequent catalytic MSR and OSR experiments. The Pd $3d_{5/2}$ signal for this preparation is typically found at ~335.8 eV. The associated Ga 3d signal is attenuated with increasing temperature due to progressive NSIP formation with Pd (i.e., the coordination of Ga with Pd increases) and shifts to lower binding energies. Between 298 and 448 K, some remaining Ga_xO_y is still visible as a broad background in the BE region ~20.5 to ~19.5 eV. This background vanishes above ~500 K due to hydrogen reduction of the oxide. For the catalytically relevant Pd_1Ga_1 NSIP tempered at 503 K, the peak maxima of the doublet are found at 18.65 eV and 19.1 eV. Regarding the valence band spectra, we note that the NSIP prepared at 503 K exhibits a considerably decreased "Cu-like" density of states (DOS) at the Fermi edge, as compared to clean Pd. The valence band series therefore reflects the expected trend of the DOS at the Fermi edge toward clean Pd at high temperatures.

3.3. Ga_2O_3–PdGa NSIP transition by hydrogen reduction

To simulate the reductive activation of Pd/Ga_2O_3 supported catalysts also on the corresponding inverse model catalysts, experiments were also conducted with Ga_2O_3 as starting material. To ensure reproducible preparation of the Ga_2O_3 overlayer and to avoid the deposition of Ga metal or Ga suboxide species, a background pressure of 10^{-3} mbar O_2 was chosen during the deposition of 4 MLE Ga to produce Ga_2O_3. This preparation leads to fully oxidized Ga_2O_3 layers, as deduced from spectral comparison with a stoichiometric Ga_2O_3 thin film reference sample, and provides a redox-defined starting point for the reduction experiments in 0.1 mbar hydrogen described in the following.

As can be seen in Fig. 4, the Pd $3d_{5/2}$ signal is initially completely screened by the multilayers of Ga_2O_3. Only above 503 K, a weak Pd signal arises at ~335.7 eV. By increasing the temperature up to ~523 K, the Pd signal gains some intensity, which is accompanied by a slight shift to higher BE's, reflecting the increased formation of a Ga-enriched NSIP surface. Above ~523 K, despite the strong increase in Pd 3d intensity, this BE trend is reversed due to the increasingly accelerated thermal dissolution of Ga into deeper Pd bulk layers. Above 523 K, the formation of a Pd_xGa_y NSIP with a peak maximum at ~18.25 eV is evident from the Ga 3d spectral region. This component increases up to 573 K and the oxide component at ~20.9 eV almost vanishes. The valence band spectra also show the decrease in the Ga-oxide component at ~5.5 eV starting at 523 K, along with the increase in the (bi-)metallic density of states at the Fermi edge. We emphasize, that the reduction/bimetallic formation temperature of ~573 K is in very good agreement with previous experiments on the reductive formation of supported Pd_2Ga bimetallic particles [11,12].

3.4. Methanol steam reforming (MSR) on Pd_1Ga_1 NSIP

To connect to the MSR measurements on the multi-layered Pd_1Zn_1 NSIP [9,10], catalytic experiments in MSR have also been conducted on multi-layered Pd_1Ga_1 NSIPs. To ensure a direct comparison, also otherwise identical experimental parameters were used. The reactor temperature was linearly ramped from 298 to 623 K (~9 K/min), and subsequently, the temperature was held isothermally at 623 K. Compositional and electronic characterization was carried out ex situ before and after the reaction by AES, LEIS and XPS, and by in situ XPS at HZB/BESSY II, respectively. The catalytic measurements were performed on model surfaces with variable Ga content. The initial Ga depositions of 1, 2 and 4 MLE ideally correspond to ~2, ~4 and ~8 layers of Pd_1Ga_1 NSIP.

Fig. 5 shows the MSR reaction rates (given in mbar/min) on the Pd_1Ga_1 NSIP prepared with 1, 2 and 4 MLE Ga. CO formation starts for all samples at roughly the same temperature (~520 K), the CO_2 formation increases at somewhat higher temperatures but remains at a very small rate in all cases (note the different scales used for the CO- and CO_2-rates in Fig. 5). An initial increase in the CO_2 formation rate at ~400 K is observed for both the 1 and the 2 MLE Ga-doped Pd_1Ga_1 NSIP, but is missing for the 4 MLE Ga-doped Pd_1Ga_1 NSIP. The reason for this feature was a minor leakage of O_2 (air) into the reactor leading to an undesired OSR low-temperature rate contribution (compare also the "controlled" OSR rates of Fig. 8), which could be finally suppressed experimentally in case of the 4 MLE experiment (lowest panel of Fig. 5). Considerable differences are notable for the formaldehyde formation. For the model catalysts with higher Ga loading, the formaldehyde increases parallel with the CO formation and the formaldehyde formation rate is higher than that of CO_2. For 2 and 4 MLE Ga, the maximum formation rates of formaldehyde are 14 and 6×10^{-3} mbar/min, also the (much higher) maximum rates of CO formation are comparable for 2 and 4 MLE Ga at ~0.20–0.25 mbar/min. In contrast, the formaldehyde formation is almost negligible for the 1 MLE Ga-prepared catalyst, but the CO formation rate is again comparable to the others at around 0.15 mbar/min. In the isothermal region all rates generally decrease due to progressive C deposition on the catalyst surface and consummation of the reactants.

The Pd_1Ga_1 NSIP with the lowest Ga loading therefore catalytically resembles a slightly modified Pd surface, since on clean Pd also no intermediate formaldehyde is detectable due to the fast dehydrogenation of HCHO to CO. Since CO, CO_2 and formaldehyde are formed in the same temperature region, but the CO_2 formation rate stays very low, all three Pd_1Ga_1 NSIP's must be considered not CO_2 selective at all and almost not capable of water activation. Depending on the Ga loading, the main benefit of the sufficiently

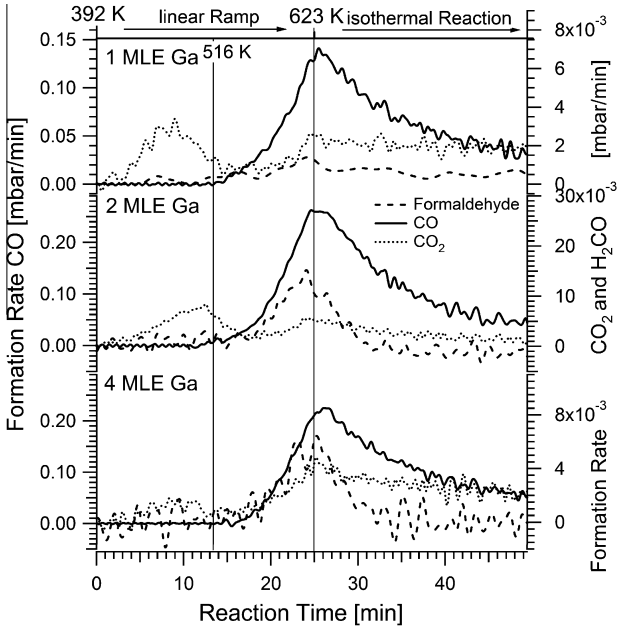

Fig. 5. Temperature-programmed MSR reaction on three different Pd_1Ga_1 NSIP's. The diagram shows, starting from the top, data of model catalysts resulting from 1, 2 and 4 MLE Ga deposition, each annealed at 503 K. Reaction conditions: 12 mbar methanol + 24 mbar water, 1000 mbar He. Linear ramp (9 K/min) up to 623 K, subsequent isothermal reaction at 623 K for 25 min (note the different scales used for the CO- and CO_2-rates). An initial increase in the CO_2 formation rate at ~400 K is observed for both the 1 and the 2 MLE Ga-doped Pd_1Ga_1 NSIP, but is missing for the 4 MLE Ga-doped Pd_1Ga_1 NSIP. The reason for this feature was a minor leakage of O_2 (air) into the reactor leading to the undesired OSR low-temperature rate contribution, which could be finally suppressed experimentally in case of the 4 MLE experiment (lowest panel). The respective TOF and product/reactant partial pressure data to Fig. 5 are shown in the Supplementary material, Figs. S2–S4.

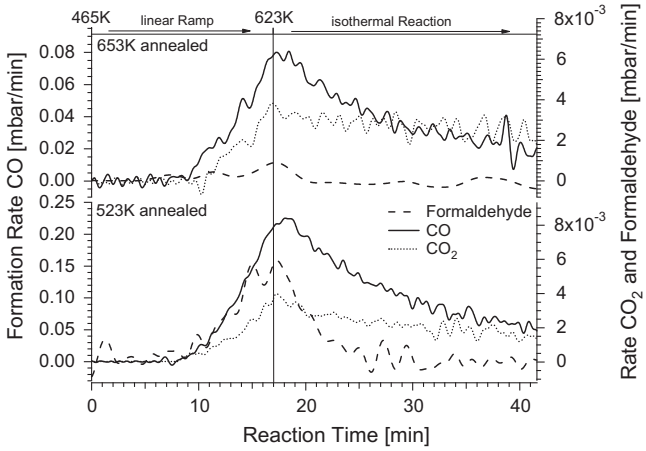

Fig. 6. Temperature-programmed MSR reaction on two differently tempered PdGa NSIP states. The diagram shows PdGa intermetallic compounds prepared with 4 MLE Ga and subsequent tempering at 653 K (upper panel) and with 4 MLE Ga and tempering at 523 K (lower panel). Reaction conditions: 12 mbar methanol + 24 mbar water, 1000 mbar He. Linear ramp (9 K/min) up to 623 K, subsequent isothermal reaction at 623 K for 25 min. The respective TOF and product/reactant partial pressure data to Fig. 6 are shown in the Supplementary material, Figs. S5–S7.

doped NSIP states therefore is a gradual promotion of more selective dehydrogenation of methanol to formaldehyde, but – despite the desired "Cu-like" electronic valence band structure (Fig. 3, right panel) – nevertheless mostly CO is formed. Furthermore, an outward corrugation of the dopant, which was shown to be related

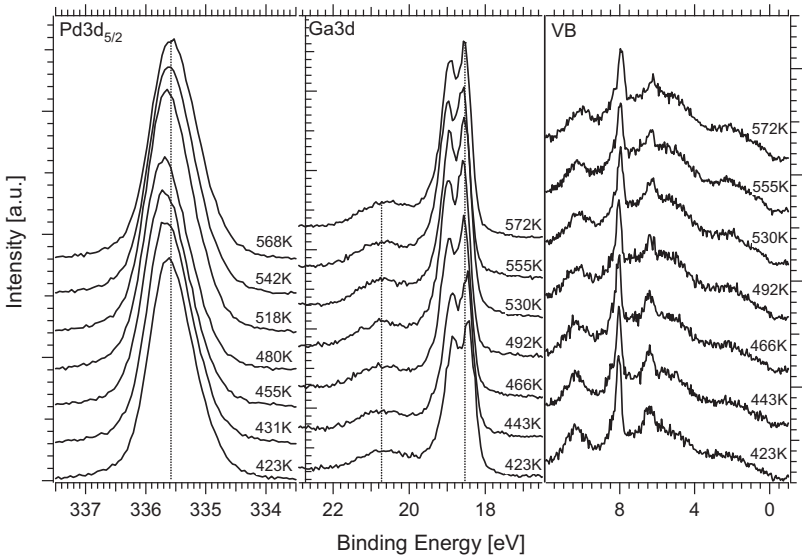

Fig. 7. Pd $3d_{5/2}$ (left), Ga 3d (middle) and valence band (right) spectra, monitored during MSR reaction starting from the 503 K-annealed 4 MLE Pd_1Ga_1 NSIP initial state. Photon energies as in Fig. 4. The spectroscopic assignment of the superimposed gas-phase valence band features is provided in the Supplementary material (Fig. S11).

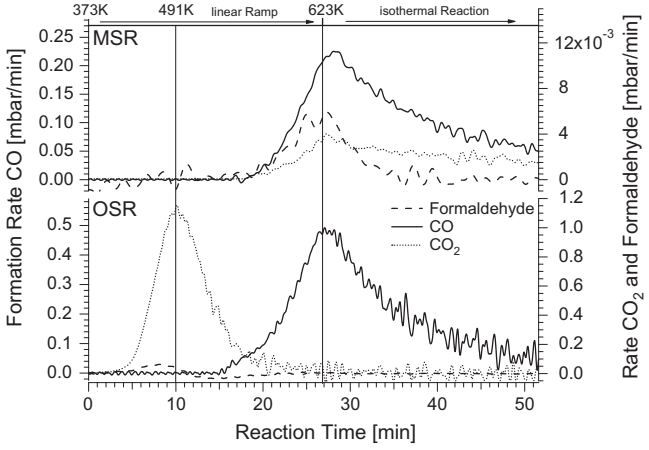

Fig. 8. Comparison of temperature-programmed MSR and OSR reaction starting from the 503 K-annealed 4 MLE Pd_1Ga_1 NSIP initial state. Reaction conditions: MSR: 12 mbar methanol + 24 mbar water, 1000 mbar He, OSR: 16 mbar methanol + 24 mbar water + 11 mbar O_2, 1000 mbar He. Linear ramp (9 K/min) up to 623 K, subsequent isothermal reaction at 623 K for 25 min. The respective TOF and product/reactant partial pressure data to Fig. 8 are shown in the Supplementary material, Figs. S8–S10.

to water activation and CO_2-selective total oxidation of intermediate formaldehyde in the PdZn case [9,10], was not observed for PdGa [22]. Assuming that only by a combination of appropriate electronic and geometric surface structure of the bimetallic the following three conditions can be met, namely

- selective dehydrogenation of methanol to formaldehyde without further reaction to CO,
- efficient water activation,
- fast and selective total oxidation of formaldehyde to CO_2,

it is obvious that at least the second condition is hardly matched by any tested Pd_1Ga_1 NSIP model system.

At this point we note that Ga_2O_3-supported bimetallic Pd_1Ga_1 particles are indeed rather CO_2-selective [11] (though not as active/selective as Pd_2Ga/β-Ga_2O_3 [11,25]), showing a ~75% selectivity around 550 K. Thus, CO formation is suppressed relative to CO_2 both in comparison with the pure β-Ga_2O_3 support and the isolated Pd_1Ga_1 NSIP, which hardly exhibits any CO_2-activity, but a lot of CO formation in the same temperature range. This strongly points to metal-support interaction playing an important role in low-temperature formaldehyde conversion, and a bi-functional synergism of both the intermetallic and the (interface to the) oxide on the supported catalyst system is quite likely.

In this context, a quantitative comparison of the rates of CO_2- vs. CO formation on our multi-layered Pd_1Ga_1 NSIP's (Fig. 5) with literature TOF data (in the following consistently given in the dimension of a reaction frequency s^{-1} *per surface site*) on model-PdZn and oxide-supported PdZn and Pd_xGa_y catalysts is useful. From the Supplementary material, the respective TOF values (Fig. S2) as well as the reactant and product partial pressures (Figs. S3 and S4) corresponding to the rate data of Fig. 5 can be read out for a given reaction time, reaction temperature and reaction conversion. Necessarily, TOF's are based on the idealized picture of a stable, static bimetallic surface exhibiting uniform Pd_1Ga_1 active surface sites throughout the entire reaction run, which is an artificial assumption for certain, surface-destabilizing reaction conditions, as well as for a "structure-sensitive" reaction proceeding preferentially at the bimetal-oxide phase boundary. In principle, the time- and temperature-resolved gas-phase partial pressure data can be used to recalculate "true" chemical reaction rates, provided that the respective individual reaction orders with respect to products and reactants were known from a fully parameterized kinetic study.

At first, lacking water activation on the bimetallic surface itself sets the Pd_1Ga_1 NSIP apart from the related multi-layered Pd_1Zn_1 NSIP, for which a CO_2-TOF of 0.04 s^{-1} (without simultaneous CO formation) was reported at ~540 K (at maximum 0.144 s^{-1} at 570 K) on the (experimentally proven) basis that a known number of surface PdZn = 1:1 ensemble sites is available, active and selective for the full MSR process [9,10]. Under otherwise identical conditions (same reaction cell and operation mode, gas-phase composition and temperature), the CO_2-TOF is below 0.0013 s^{-1} at 540 K in the present PdGa case (4MLE Ga sample). Because the "uniform" bimetallic 1:1 PdGa surface sites are hardly MSR/CO_2-active, likely only some special active centers (of unknown number and nature) contribute to the maximum CO_2 formation rate of

0.012 s^{-1} measured at 623 K in parallel with strong CO formation. Since CO, which has been recently shown to destabilize the intermetallic surface of Pd_2Ga particles [25], is already present in the gas phase in substantial amounts (~0.8 mbar), and also the thermal decay of the NSIP is proceeding (see Fig. 3), it is even more doubtful to assign this (rather small) CO_2 activity to the total number of initially present PdGa surface ensembles.

Likely because of facilitated water activation both the supported PdZn and Pd_2Ga catalysts exhibit a much broader temperature range with high CO_2 selectivity and activity, due to improved conversion of the intermediate formaldehyde toward CO_2, and generally become active for methanol conversion at considerably lower temperatures (below 490 K) than the "isolated" bimetallics (~520 K). CO_2-TOF's of 0.17 s^{-1} on a supported PdZn/ZnO and of 0.06 s^{-1} on a Pd_xGa_y/Ga_2O_3 catalyst were reported at 493 K reaction temperature by Takezawa and Iwasa [1]. Ranganathan et al. reported 0.8 s^{-1} at 503 K [26] and Conant et al. 0.39 s^{-1} at 523 K [27], both for PdZn/ZnO.

The above-mentioned study by Haghofer et al. [25] moreover allows to compare our CO-TOF's with those deduced for supported Pd_2Ga particles. These are reportedly affected by partial (surface-near) Pd metal segregation, induced by the MSR reaction environment. A methanol conversion TOF of 0.08 s^{-1} is reported at 523 K, corresponding to a CO-TOF of 0.008 s^{-1} (~10% CO selectivity). By fitting our CO-TOF data (Fig. S2) with a simple Arrhenius rate function in the temperature region 480 K-580 K, the CO-TOF's at 523 K on the 1,2 and 4 MLE Pd_1Ga_1 NSIP's can be recalculated also for the low rate values at 523 K, yielding CO-TOF values around 0.015 s^{-1}, respectively. This TOF comparison is somewhat more straightforward because the unwanted "full" methanol dehydrogenation toward CO is likely "structure insensitive", that is, largely takes place at the bimetallic surface itself, which may be comparably "gas-phase-disturbed" also under our conditions. As the CO-TOF's are similar, we may derive additional support for the blocking of the low-temperature CO_2-forming reaction channel on the "isolated" intermetallic surface.

To corroborate the formaldehyde-stabilizing role of the multilayered Pd_1Ga_1 NSIP, Fig. 6 shows similar MSR experiments for a 4 MLE Ga-doped Pd_1Ga_1 NSIP tempered to 523 K and a 4 MLE Pd_1Ga_1 NSIP sample tempered to much higher temperature, that is, 653 K. Again, the TOF values corresponding to Fig. 6, as well as the respective reactant- and product partial pressures can be read out in the Supplementary material (Figs. S5–S7) for a given reaction time, reaction temperature and reaction conversion. The methanol conversion starts at ~520 K and shows similar maximum rates for product formation on both model systems. The dominant CO formation starts in the same temperature region. However, the maximum rate of CO formation is almost doubled on the 523 K-tempered sample, compared to the 653 K-annealed NSIP. The main difference is noted in the formaldehyde formation rates. On the multilayer Pd_1Ga_1 NSIP with a lower tempering temperature, and therefore, a higher Ga content in the top-most layers, the formation of formaldehyde starts in parallel with CO formation and the maximum rate is higher than that of CO_2, whereas formaldehyde is almost completely suppressed on the 653 K-tempered sample. Again, the maximum rates of CO and CO_2 formation are found at around 623 K. In the isothermal region, once again deactivation processes and reactant consumption attenuate the reaction rates. In summary, in no case a PdZn-analogous CO_2-selective low temperature region has been observed under MSR conditions. We note that the measurements on the 653 K-tempered sample and the PdGa sample with 1 MLE Ga (cf. Fig. 5) very much resemble each other, pointing to the presence of a rather thin, and thus more strongly Pd-coordinated and thus catalytically more "Pd-like", PdGa NSIP state in both cases.

3.5. In situ XPS measurements under MSR reaction conditions

To gain full insight into the redox changes on the Pd_1Ga_1 NSIP under MSR conditions, the associated in situ XPS experiments have been also conducted at HZB/BESSY II under comparable conditions on the 4 MLE Ga-doped and 523 K-annealed Pd_1Ga_1 NSIP (cf. 523 K – spectra of Fig. 3 for the pre-reaction state).

Fig. 7 shows the related in situ XPS data in a reaction mixture of 0.12 mbar methanol + 0.24 mbar water. Hardly any spectral changes can be seen in the observed temperature range ~423–570 K in all presented spectral regions. This especially applies to the temperature-invariant oxide component at ~20.7 eV, which almost remains constant in intensity, showing that initially occurring partial surface segregation of oxidized Ga species is basically finished already at around 423 K, and no additional reaction-caused oxide segregation is thereafter observed. The Pd $3d_{5/2}$ signal even shows a small shift to higher BE's between 431 and 518 K, which again confirms the high thermochemical stability of the Pd_1Ga_1 NSIP under MSR conditions. As a consequence, the Pd_1Ga_1 NSIP on the one hand represents a highly stable model system, but on the other hand hardly is appropriate to model the MSR catalytic properties of the oxide-supported nano-particulate bulk intermetallic compound phases, at least in its purely bimetallic state.

3.6. Oxidative methanol steam reforming on Pd_1Ga_1 NSIP

3.6.1. Catalytic experiments

Analogous experiments in oxidative steam reforming (OSR) have been additionally performed. The reaction conditions are similar to those of the MSR reaction, with the one exception of O_2 being admitted before the reaction (ratio methanol/water/oxygen ~1:2:0.7). Adding a certain partial pressure of oxygen to a methanol–water feed is common to match two requirements: firstly, to compensate for the endothermicity of the "pure" MSR reaction ("autothermal reforming") and secondly, to additionally suppress the CO concentration in the product stream via enhanced CO oxidation. Fig. 8 (lower panel) highlights the OSR reaction rates (given in mbar/min) measured on a 4 MLE Ga, 523 K-annealed Pd_1Ga_1 NSIP. For a better comparison, the upper panel shows the analogous MSR reaction run in the absence of O_2. From the Supplementary material (Figs. S8–S10), the respective reactant and product partial pressures as well as the respective TOF values can be deduced for a given reaction time, reaction temperature and reaction conversion (the TOF's are based on the idealized picture of a stable bimetallic surface exhibiting uniform Pd_1Ga_1 active surface sites throughout the entire reaction run).

The most notable difference to the MSR reaction without added O_2 is the very high CO_2 formation rate setting in already at low temperatures (~423 K). The maximum rate of CO_2 formation is achieved at around 491 K with 1.2 mbar/min, which is almost three orders of magnitude higher than under MSR conditions (4×10^{-3} mbar/min), and even higher than the maximum CO formation rate (~0.48 mbar/min) observed in the same experiment at around 623 K. In parallel with CO_2 formation, formaldehyde formation sets in, but at a much smaller rate (~0.05 mbar/min at maximum). Interestingly, a period of deactivation at ~550 K is evident after about 16 min of reaction, which is mainly due to quantitative oxygen consumption from the reaction mixture. CO formation starts at ~530 K, and the maximum rate is reached at 623 K (~0.48 mbar/min). In the isothermal region, the CO formation decreases to less than 0.05 mbar/min due to almost quantitative consumption of the initial methanol amount in the batch reactor.

The time-resolved H_2-mass balance of the OSR reaction run of Fig. 8 has been precisely determined by continuous measurement of the H_2-amount as a function of reaction time and –temperature and is also represented graphically in the Supplementary material (Fig. S10). During the oxygen-consuming reaction, which extends up to a temperature of ~550 K, about 87% of the converted methanol is totally oxidized to CO_2 and water, and only a minor 13% contribution of partial oxidation toward CO_2 and H_2 is observed. In conclusion, only this minor fraction of the methanol becomes partially oxidized, according to the reaction stiochiometry $CH_3OH + 1/2\ O_2 \rightarrow CO_2 + 2H_2$. Nevertheless, this proves that a reaction pathway for a hydrogen-producing reaction even in the simultaneous presence of O_2 is possible and that total oxidation according to the stoichiometry $CH_3OH + 3/2\ O_2 \rightarrow CO_2 + 2H_2O$ does not take place exclusively. Moreover, the very high CO_2-selectivity in the temperature range around 500 K indicates that O_2 addition could indeed be helpful to optimize CO_2 selectivity and to efficiently suppress the CO content of the reformate gas also under continuous flow reaction conditions.

In summary, a highly CO_2 selective, combined total/partial oxidation reaction was obtained under OSR conditions in the temperature region ~420–520 K, in strong contrast to MSR.

In conclusion, the Pd_1Ga_1 NSIP is capable of efficiently activating oxygen at low temperatures, while being inactive for CO formation at the same time. Methanol is converted to CO_2 mainly via total oxidation of intermediary formed C_1-oxygenates at the surface with some simultaneous hydrogen production. Since we are not aware of methanol total or partial oxidation TOF's measured on any of the literature-reported PdGa or PdZn systems, a comparison of the OSR rates between model and real systems is currently not possible.

3.6.2. In situ XPS experiments under OSR conditions and the influence of O_2 on the dynamical redox state of the catalyst

The in situ XPS experiments were performed in close experimental analogy to the OSR batch reactor measurements of Section 3.6.1 to ensure a reliable correlation of the results. As the measurements at HZB/BESSY II were performed under flowing conditions, "switching" experiments with defined admission and removal of oxygen were additionally feasible without interrupting the reaction. These experiments allowed a direct evaluation of the oxidation potential of the gas phase on the dynamical redox state of the catalyst surface.

Fig. 9 depicts the spectroscopic results (Pd $3d_{5/2}$, Ga 3d and valence band regions) of the temperature-programmed OSR reaction on the 4 MLE Ga 503 K-annealed Pd_1Ga_1 NSIP. After tempering, but before start of the OSR reaction, the Pd $3d_{5/2}$ peak maximum is found at ~335.9 eV and the Ga 3d signal only shows the Pd_1Ga_1 NSIP contribution, but no oxidic contribution. Also the valence band shows only fingerprints of the multilayer Pd_1Ga_1 NSIP. After admission of the O_2-containing reaction mixture and slight increase in the reaction temperature (~365 K), the peak maximum of the Pd peak shifts to slightly lower BE's, but still stays in the range of a typical Pd_1Ga_1 NSIP (~335.8 eV; to be compared to 336.0 eV for bulk Pd_1Ga_1 [23] and to 335.6 eV for bulk Pd_2Ga [24]). The valence band region now shows also the gas-phase signals of the reactant mixture (the spectroscopic assignment of the individual gas-phase contributions is provided in the Supplementary material (Fig. S11)). The Ga 3d signal shows the development of an oxidized Ga component at ~20.4 eV, which reaches its maximum intensity at 464 K, that is, slightly below the temperature where the maximum of the CO_2 formation rate is observed (491 K, cf. Fig. 8).

By correlation of the relative intensity trend of the Ga(ox) component with the catalytic selectivity pattern, this component is apparently linked to highly selective CO_2 formation. The nature and potential catalytic function of the related oxidized Ga species (active vs. spectator, etc.) is nevertheless unclear at present. Anything in between Ga–O(ads) on intact Pd_1Ga_1 sites, resulting from "simple" dissociative O_2 adsorption on the persisting intermetallic surface, and local/partial oxidative segregation giving rise to more- or less-extended two-dimensional Pd-ensembles and nearby Ga (hydr)oxide islands is conceivable. According to the depth profiling information of Fig. 10, the oxidized Ga species detected at ~500 K is rather "flat" (estimated thickness ~0.5 nm, based on the relative intensity change of bimetallic vs. oxidized Ga observed between 120 eV and 650 eV photon energy) and situated in close vicinity of a still stable surrounding intermetallic environment (compare Pd $3d_{5/2}$ BE maximum at 335.8 eV at 460–500 K). Thus, extended oxidative decomposition of the model surface into three-dimensional

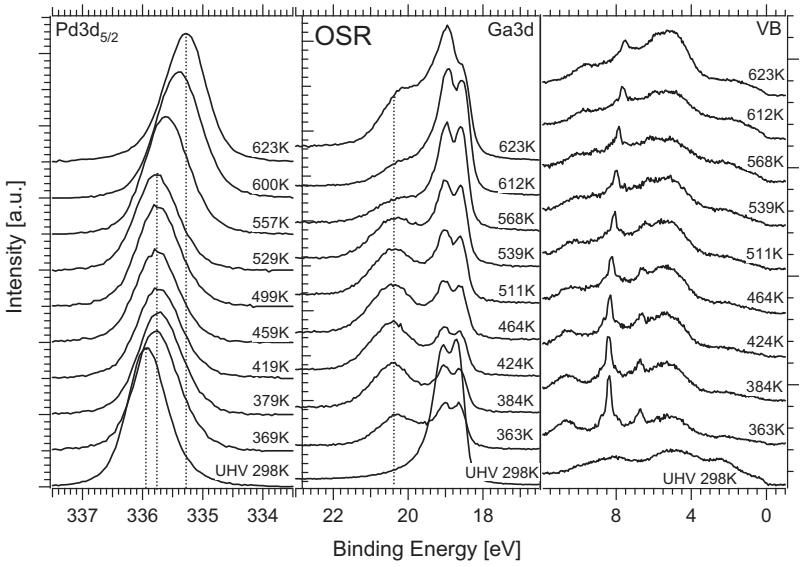

Fig. 9. Pd $3d_{5/2}$ (left), Ga 3d (middle) and valence band (right) spectra, taken during OSR reaction (ratio methanol/water/oxygen = 1:2:0.5, total pressure 0.25 mbar), starting from the 503 K-annealed 4 MLE Pd_1Ga_1 NSIP initial state. Photon energies were the same as in Fig. 4. The "initial state" spectra at 298 K were collected immediately before admission of the gas mixture. The spectroscopic assignment of the superimposed gas-phase valence band features is provided in the Supplementary material (Fig. S11).

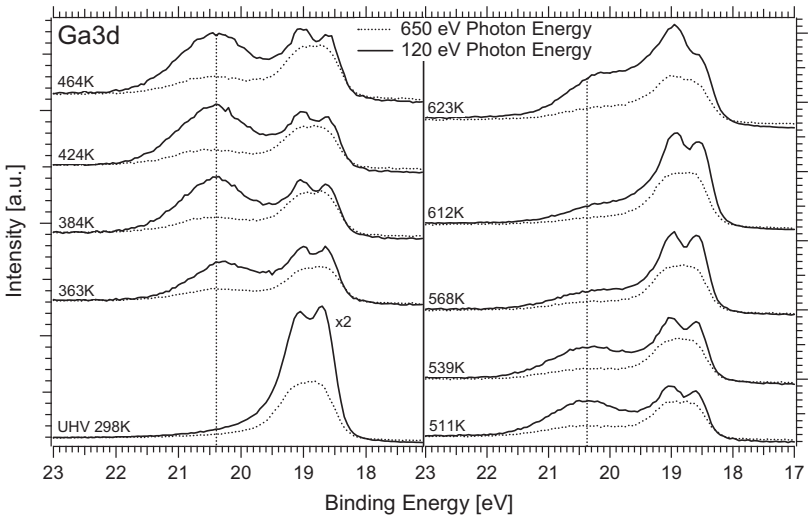

Fig. 10. Direct comparison of the Ga 3d signals taken during OSR reaction (reaction conditions as in Fig. 10) and measured with 120 eV and 650 eV photon energies, respectively. To visualize the rather small Ga_2O_3 intensity of the 298 K spectra, both were increased by a factor of 2.

Pd metal and Ga_2O_3 domains can be excluded at least at around 500 K.

The shift of the Pd $3d_{5/2}$ signal remains constant up to ~529 K at the value typical for the Pd_1Ga_1 NSIP. Only at higher temperatures (557–623 K) a pronounced shift to 335.25 eV due to extended oxidative decomposition of the NSIP toward three-dimensional Pd metal is observed, which coincides with increasing CO formation in Fig. 8 (lower panel). This trend is also reflected in the Ga 3d signal. From 539 to 612 K, the Ga bimetallic component at ~18.4 eV gains intensity relative to the oxidic component at ~20.4 eV. This could be explained by the rearrangement of the two-dimensional, partially oxidized Ga layer to three-dimensional Ga-oxide islands, accompanied by extended formation of areas of clean Pd, which in turn progressively catalyze formation of CO. From 612 to 623 K the oxide component again gains very much intensity, which can be explained by extra Ga_2O_3 segregation from deeper Ga layers, corresponding to more or less complete thermal/oxidative destruction of the NSIP. This interpretation is also consistent with the strong shift of the Pd 3d signal toward the Pd metal typical value of 335.25 eV. The related valence band spectra show increased formation of oxidic components at 4–5 eV at 623 K and an increase in the DOS at the Fermi edge typical for metallic Pd.

During the OSR reaction, we monitored not only the surface-sensitive Ga 3d Signal at a photon energy of 120 eV, but also a corresponding signal at 650 eV photon energy in order to gain information about the vertical distribution of the different Ga species. Fig. 10 shows that the CO_2-active oxidized Ga species, which has been formed during the reaction at <540 K, is found mainly as a "wetting" species (average thickness ~0.5 nm, see above) in the topmost layer of the model catalyst. For all temperatures below 540 K, the change of the photon energy from 120 to 650 eV thus results in a strong relative decrease in the oxide component compared to the bimetallic component, for example, at 464 K from 3:2 to 1:3. In contrast, the oxide species segregated at temperatures above 540 K appears to grow in thickness, as inferred from a less depth-dependent ratio of the components at different photon energies (e.g., at 623 K 2:3 and 1:2 at 120 and 650 eV). This strongly supports our interpretation of increased three-dimensional segregation of unreactive gallium oxide on an already Pd-like metal surface above 540 K.

Summarizing, the results indicate a thermochemical stability limit of the Pd_1Ga_1 NSIP at around 540 K under OSR conditions, in contrast to the clean MSR reaction, where a higher stability limit has been verified. In the batch reactor OSR experiment of Fig. 8, quantitative O_2 consumption and degradation of the initial NSIP state coincide at this limit, thus the pronounced transition from CO_2- to CO formation is observed.

In order to study the dynamic response of the catalyst surface to the change of the gas-phase oxidation potential, we additionally performed experiments with deliberate on/off switching of oxygen, that is, between MSR and OSR conditions, again starting from the 503 K-annealed 4 MLE Pd_1Ga_1 NSIP. Fig. 11 shows these comparative experiments at three selected reaction temperatures. The Pd $3d_{5/2}$ signal is found at ~335.7 eV at 463 K ("CO_2-active" state in OSR, compare Fig. 8). The change between MSR and OSR conditions obviously has no measurable effects on the BE of Pd at around 463 K (NSIP largely stable). The Ga 3d signal, however, shows a reversible decrease/increase in the oxidized Ga component (~20.2 eV) upon switching between OSR and MSR. This means that the "wetting" Ga(ox) species exhibits a fast "kinetic" response to the gas phase and thus exhibits pronounced methanol-induced reducibility in the absence of O_2 (in parallel, the valence band spectra exhibit a change in the gas-phase signals (e.g., at ~8 eV) due to the altered composition and ionization probability of the gas phase, see Supplementary material Fig. S11). When the reaction temperature is increased to 523 K under OSR conditions (close to the "inactive state" in Fig. 8), the Pd $3d_{5/2}$ signal already exhibits a shift to a Pd-like BE (~335.35 eV). In accordance, the DOS at the Fermi edge is increased. Switching between MSR and OSR again causes no significant changes in the Pd signal. Partially reversible alterations in the Ga 3d signal (decrease in the oxidized Ga component when switching off O_2) are still observed. If the reaction temperature is then raised under MSR conditions to 573 K ("CO-active" state), the oxidic component in the Ga 3d signal vanishes completely due to the increased reductive potential of the gas phase. We note that complete reduction toward the intermetallic state at this temperature is necessarily connected with fast Ga loss into deeper bulk layers occurring in parallel with reduction. The Pd $3d_{5/2}$ signal again remains constant at 335.35 eV. Only upon switching to OSR conditions, the Pd signal shifts to even lower BE's (~335.2 eV) due to additional Ga-depletion of Pd by oxidative Ga segregation combined with simultaneous Ga bulk diffusion. Again, the oxidic component in the Ga 3d signal appears in the presence of O_2. Taken together, this indicates almost complete

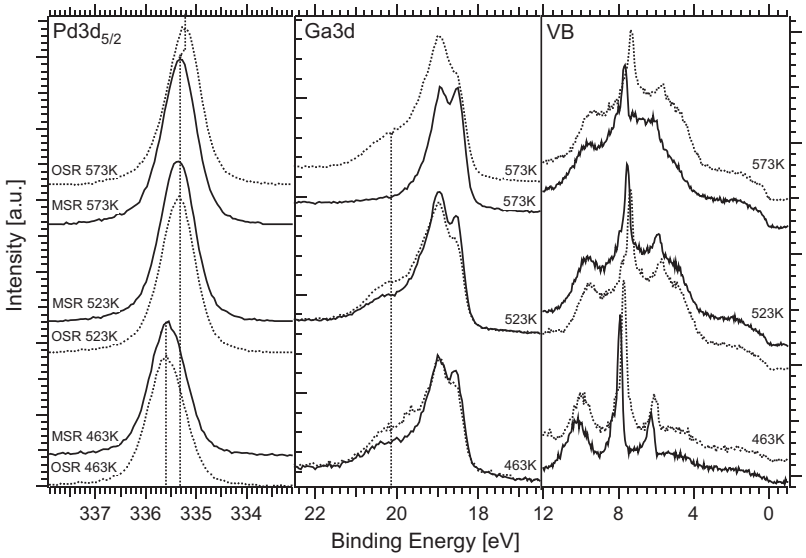

Fig. 11. Pd $3d_{5/2}$ (left), Ga 3d (middle) and valence band (right) spectra, taken at 463 K, 523 K and 573 K during switching from MSR (ratio methanol/water 1:2, total pressure 0.26 mbar) to OSR conditions (ratio methanol/water/oxygen 1:2:0.5, total pressure 0.31 mbar). Initial catalyst state: 503 K-annealed 4 MLE Pd_1Ga_1 NSIP. Photon energies as in Fig. 3. The spectroscopic assignment of the superimposed gas-phase valence band features is provided in the Supplementary material (Fig. S11).

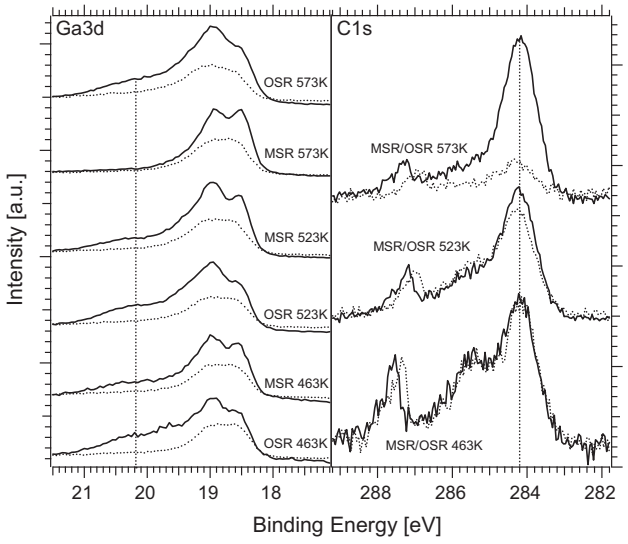

Fig. 12. Direct comparison of the Ga 3d signals taken during OSR and MSR reaction at three different reaction temperatures (463 K, 523 K and 573 K) with variable photon energy at 120 eV (solid line) and 650 eV (dotted line). The right panel shows the C 1s spectra taken at 410 eV photon energy (dotted – OSR, solid – MSR). Initial catalyst state: 503 K-annealed 4 MLE Pd_1Ga_1 NSIP.

oxidative decomposition of the multilayer Pd_1Ga_1 NSIP at ~573 K. The DOS at the Fermi level is also strongly altered and now exhibits the shape of clean Pd.

A reversible dynamic response is therefore proven for all three reaction temperatures, with the strongest response at 573 K. At this temperature, Fig. 4 already indicated the reductive formation of an intermetallic surface layer from pre-formed stoichiometric Ga_2O_3. In presence of a variable oxygen pressure this process can be driven almost fully reversible. However, the so-prepared Pd_xGa_y NSIP surfaces strongly favor methanol dehydrogenation toward CO due to their electronic similarity to clean Pd and the dominant three-dimensional oxide segregation.

Fig. 12 finally shows that the changes observed during the switching from MSR to OSR around 463 K mainly affect the top-most surface layers. The oxide component of the Ga 3d signal is attenuated in deeper layers (ratio of oxidized Ga to bimetallic Ga 3:7 vs. 1:4 at 120 eV vs. 650 eV photon energy). At the highest temperatures (573 K), the decomposition of the multilayer Pd_1Ga_1 NSIP to three-dimensional oxide segregation is increasingly evident (ratio of oxidized to bimetallic Ga 3:7 vs. 3:7 at 120 vs. 650 eV photon energy). The in-parallel recorded C1s signal shows that at 463 K and 523 K reaction temperature almost the same amount of carbon is present on the surface under both MSR and OSR conditions. At 573 K a strong decrease in the C 1s signal indicates reactive removal of carbon by O_2 in course of full NSIP decomposition toward the Pd-like surface.

4. Conclusions

We have shown that in close analogy to the Pd_1Zn_1 NSIP system, preparation by deposition of several MLE Ga and thermal annealing at ~523 K leads to analogous multi-layered Pd_1Ga_1 NSIP states.

In contrast to MSR measurements on supported Pd_1Ga_1/β-Ga_2O_3, Pd_2Ga/β-Ga_2O_3, and on the related Pd_1Zn_1 NSIP, which all showed increased CO_2 selectivity at $T \leqslant 550$ K, the multi-layered Pd_1Ga_1 NSIP is a poor, unselective catalyst in MSR, as evidenced by simultaneous, unselective production of mainly CO, little CO_2 and some HCHO in parallel in the same temperature region. Nevertheless, it is highly CO_2 selective and active in the presence of O_2. The most likely explanation is that water activation on the NSIP is not working, but O_2 activation works well, so in MSR, the required "source of oxygen" for total oxidation of C_1 intermediates is missing but becomes available under OSR conditions. The H_2-mass balance of the OSR around 500 K, moreover, implies that once a "source of oxygen" is available, also some (partial) reforming ability of the intermetallic surface toward CO_2 and H_2 is established already at low temperatures. For the (relative to the Pd_1Ga_1 NSIP) considerably more CO_2-active supported Pd_1Ga_1 system [11] we thus rather suspect a water-splitting role of the bimetal-oxide phase boundary and/or its oxidic catchment area than an intrinsic ability of the intermetallic surface itself to perform full reforming including water splitting. This distinguishes the 1:1 PdGa NSIP also from the 1:1 PdZn NSIP, for which a bi-functional, water-activating role of "isolated" bimetallic surface ensembles was verified in Refs. [9,10].

Obviously, for the supported PdGa system it is important to consider the role of the support and the formation of suitable metal-oxide interfacial sites capable of water activation. A bi-functional synergism therefore rather applies to the bimetallic/oxide interface than to a regular, ordered array of active sites on the bimetallic surface itself. This is also corroborated by in situ XPS measurements under MSR reaction conditions, which revealed that the NSIP did neither structurally nor chemically change during the MSR runs. Especially, no signs of water-induced surface oxidation of the NSIP were observed, in contrast to the analogous Pd_1Zn_1 NSIP.

Only under in situ OSR conditions, "wetting" Ga(ox) species are reversibly formed/segregated and this segregation process is obviously important for the combined total/partial oxidation of C_1-oxygenate intermediates (HCHO, CO, etc.) to CO_2. Mechanistically, it remains unclear whether the formation of (even very small/thin) Pd-ensembles favors full dehydrogenation of methanol toward CO(ads), followed by oxidation of CO by O(ads) toward CO_2, or whether the total oxidation/CO_2-formation propensity of the Pd_1Ga_1 NSIP around 500 K represents an intrinsic property of the intact Pd_1Ga_1 surface. If, for example, minor partial oxidative segregation was limited to the top layer of the original NSIP, changes to the mean Ga coordination of top-layer Pd atoms should be minor, too, which could somehow explain the rather stable 1:1 NSIP binding energy position of the Pd3d signal around 500 K during OSR. Partial, near-surface oxidative decomposition in the presence of either CO or O_2 already at low temperatures has been recently shown in an in situ PM-IRAS and XPS study of ambient-pressure gas-phase effects on Ga_2O_3-supported Pd_2Ga particles [25]. Some shortcomings of the NSIP approach have to be admitted: the 1:1 PdGa NSIP, although multi-layered, does not represent an unambiguous model for the surface of Pd_1Ga_1 nanoparticles or bulk compounds, although the XPS-observed VB electronic structure after ~503 K annealing is representative for the expected "Cu-like" electronic situation favoring selective methanol dehydrogenation toward HCHO. So far, no direct structural analogies between the ~4 and 8 layers thick model NSIP (Pd-like, substitutional fcc structure) and the related 1:1 PdGa bulk intermetallic compound (FeSi-structure) could be verified.

Unfortunately it was also not possible to prepare a bulk-analogous Pd_2Ga NSIP, which would represent a more suitable "purely bimetallic" model system for the most selective Pd_2Ga nanoparticles. A common reasoning for the (relative to Pd_2Ga/β-Ga_2O_3) lowered CO_2-selectivity of both supported and unsupported Pd_1Ga_1 might be related to either an intrinsically low selectivity of the "static" bimetallic surface itself or, as suspected in Ref. [11], to pronounced oxidative segregation of Ga under reaction conditions. Analogous experiments both on bulk PdGa and Pd_2Ga compounds and on clean Pd are presently under way to fully clarify the situation.

Acknowledgments

This work was financially supported by the Austrian Science Fund through Grants P20892-N19 and SFB F4503-N16. Ch. Rameshan acknowledges a PhD scholarship granted by the Max-Planck Society. Support for the measurements at HZB/BESSY II was granted through EU Program RII3-CT-2004-506008, Proposal No. 2008_2_80336. The authors thank the BESSY staff for their support of the in situ XPS measurements.

Appendix A. Supplementary material

Supplementary data associated with this article can be found, in the online version, at http://dx.doi.org/10.1016/j.jcat.2012.03.009.

References

[1] N. Takezawa, N. Iwasa, Top. Catal. 22 (2003) 215.
[2] T. Iwasa, T. Mayanagi, W. Nomura, M. Arai, N. Takezawa, Appl. Catal. A 248 (2003) 153.
[3] D.R. Palo, R.A. Dagle, J.D. Holladay, Chem. Rev. 107 (2007) 3992.
[4] A. Bayer, K. Flechtner, R. Denecke, H.P. Steinruck, K.M. Neyman, N. Rösch, Surf. Sci. 600 (1) (2006) 78–94.
[5] H. Gabasch, A. Knop-Gericke, R. Schlogl, S. Penner, B. Jenewein, K. Hayek, B. Klötzer, J. Phys. Chem. B 110 (23) (2006) 11391–11398.
[6] K.M. Neyman, K.H. Lim, Z.X. Chen, L.V. Moskaleva, A. Bayer, A. Reindl, D. Borgmann, R. Denecke, H.P. Steinruck, N. Rosch, Phys. Chem. Chem. Phys. 9 (27) (2007) 3470–3482.
[7] A. Karim, T. Conant, A. Datye, J. Catal. 243 (2006) 420;
A Karim, T. Conant, A. Datye, PhysChemChemPhys 10 (2008) 5584;
M.P. Hyman, V. Lebarbier, Y. Wang, A. Datye, J. Vohs, J. Phys. Chem. C 113 (2009) 7251.
[8] M. Kratzer, A. Tamtogl, J. Killmann, R. Schennach, A. Winkler, Appl. Surf. Sci. 255 (11) (2009) 5755–5759.
[9] C. Rameshan, C. Weilach, W. Stadlmayr, S. Penner, H. Lorenz, M. Hävecker, R. Blume, T. Rocha, D. Teschner, A. Knop-Gericke, R. Schlögl, D. Zemlyanov, N. Memmel, G. Rupprechter, B. Klötzer, J. Catal. 276 (1) (2010) 101–113.
[10] C. Rameshan, W. Stadlmayr, C. Weilach, S. Penner, H. Lorenz, M. Havecker, R. Blume, T. Rocha, D. Teschner, A. Knop-Gericke, R. Schlogl, N. Memmel, D. Zemlyanov, G. Rupprechter, B. Klötzer, Angew. Chemie-Intl. Ed. 49 (18) (2010) 3224–3227.
[11] H. Lorenz, S. Penner, W. Jochum, C. Rameshan, B. Klötzer, Appl. Catal. A 358 (2) (2009) 203–210.
[12] S. Penner, H. Lorenz, W. Jochum, M. Stoger-Pollach, D. Wang, C. Rameshan, B. Klötzer, Appl. Catal. A 358 (2) (2009) 193–202.
[13] J. Osswald, Dissertation, Technische Universität Berlin, 2006.
[14] B. W. Jaskula, in: Mineral Commodity Summaries, Reston, USA, 2011.
[15] D. El Allam, M. Gaune-Escard, J.-P. Bros, E. Hayer, Metall. Mater. Trans. B 23 (1992) 39–44.
[16] K. Kovnir, M. Armbrüster, D. Teschner, T.V. Venkov, F.C. Jentoft, A. Knop-Gericke, Yu. Grin, R. Schlögl, Sci. Technol. Adv. Mater. 8 (2007) 420.
[17] B.H. Verbeek, P.K. Larsen, W.M. Gerits, Vacuum 33 (10–12) (1983) 813–814.
[18] M. Armbrüster, K. Kovnir, M. Behrens, D. Teschner, Y. Grin, R. Schlögl, J. Am. Chem. Soc. 132 (2010) 14745–14747.
[19] T. Shido, Y. Iwasawa, J. Catal. 129 (1991) 343;
W. Jochum, S. Penner, R. Kramer, K. Föttinger, G. Rupprechter, B. Klötzer, J. Catal. 256 (2008) 278.
[20] W. Reichl, G. Rosina, G. Rupprechter, C. Zimmermann, K. Hayek, Rev. Sci. Instrum. 71 (3) (2000) 1495–1499.
[21] H. Bluhm, M. Havecker, A. Knop-Gericke, E. Kleimenov, R. Schlogl, D. Teschner, V.I. Bukhtiyarov, D.F. Ogletree, M. Salmeron, J. Phys. Chem. B 108 (38) (2004) 14340–14347.
[22] W. Stadlmayr, B. Klötzer, S. Penner, N. Memmel, in press.
[23] K. Kovnir, M. Armbrüster, D. Teschner, T. Venkov, L. Szentmiklósi, F.C. Jentoft, A. Knop-Gericke, Yu. Grin, R. Schlögl, Surf. Sci. 603 (2009) 1784–1792.
[24] K. Kovnir, D. Teschner, M. Armbrüster, P. Schnörch, M. Hävecker, A. Knop-Gericke, Yu. Grin, R. Schlögl, BESSY Highlights, 2007, pp. 22–23.
[25] A. Haghofer, K. Föttinger, F. Girgsdies, D. Teschner, A. Knop-Gericke, R. Schlögl, G. Rupprechter, J. Catal. 286 (2012) 13–21.
[26] E.S. Ranganathan, S.K. Bej, L.T. Thompson, Appl. Catal. A 289 (2005) 153–162.
[27] T. Conant, A.M. Karim, V. Lebarbier, Y. Wang, F. Girgsdies, R. Schlögl, A. Datye, J. Catal. 257 (2008) 64–70.